Scaling of Hydrophobic Solvation Free Energies[†]

David M. Huang, Phillip L. Geissler, and David Chandler*

Department of Chemistry, University of California at Berkeley, California 94720

Received: January 31, 2001; In Final Form: April 3, 2001

We have calculated the free energy of solvation for hard sphere solutes, as large as 20 Å in diameter, in two simple-point-charge models of water. These results were obtained using umbrella sampling of ensembles with fixed, ambient temperature and pressure. For the same water models, we have also calculated the surface tension of a liquid−vapor interface at room temperature. Analogous calculations were carried out for three thermodynamic states of the Lennard-Jones (LJ) fluid near liquid−vapor coexistence. For both water and the LJ fluid at the conditions we have simulated, extrapolation of our results suggests that the planar interface between coexisting liquid and vapor phases has the same surface tension as the planar limit of hard sphere solvation. We expect this correspondence to be a general result for fluids at thermodynamic states close to phase coexistence, as measured by the difference in chemical potential between bulk liquid and vapor phases, and far from the critical point. The solvation free energies we have computed for water and the LJ fluid cross over at microscopic solute sizes from a dependence on solute volume to an approximate dependence on solute surface area, as predicted by Lum et al. [*J. Phys. Chem. B* **1999**, *103*, 4570].

I. Introduction

Recent work has highlighted the existence of a crossover in the dependence of hydrophobic solvation upon solute size:[1] Accommodation of a small hard sphere (the ideal hydrophobic solute) in simulated liquid water is governed by solvent density fluctuations that closely obey Gaussian statistics.[2−4] The excess free energy of solvation, $\Delta\mu$, scales approximately with the solute's volume in this case. For very large solutes, on the other hand, water molecules near the solute experience a strong net attraction toward the bulk. Because water at ambient conditions is not far from liquid−vapor coexistence, significant solvent depletion, or drying, then occurs at the surface of the solute, as anticipated long ago by Stillinger.[5] In this case, $\Delta\mu$ is dominated by interfacial free energetics and should scale with the solute's surface area. A crossover thus exists in $\Delta\mu(R)$ as a function of solute radius R.[1] Many phenomena, such as protein folding, involve hydrophobic regions of widely varying length scales. For such processes, the crossover in $\Delta\mu(R)$ as a function of R is expected to have important implications.[6]

In the present work, we establish details of the crossover in $\Delta\mu(R)$, using Monte Carlo simulations of SPC[7] and SPC/E[8] models of water at fixed temperature and pressure. By effectively growing cavities in water reversibly, as described in section II A, we have determined the range of solute sizes at which the crossover occurs, as well as the asymptotic behavior of $\Delta\mu(R)$ for large R. These details have not been provided by previous simulations[9−17] because sufficiently large hydrophobic solutes have not been considered.

At liquid−vapor phase coexistence, the presence of a large hydrophobic surface will nucleate a vapor phase. In this case, the surface contribution to $\Delta\mu(R)$ scales asymptotically as $4\pi\gamma R^2$, where γ is the surface tension of the corresponding liquid−vapor interface. In contrast, away from coexistence, the distribution of solvent molecules around the solute differs from the structure of a liquid−vapor interface, and interfacial fluctuations may be inhibited by a rigid solute. The effective surface tension of the solute in this case, $\tilde{\gamma}$, may therefore deviate from γ. Water at standard conditions is close to but not at phase coexistence. The distinction between γ and $\tilde{\gamma}$ for this substance is thus worthy of consideration. Here, we refer to a fluid "close to coexistence" as one in which the difference in chemical potential between metastable vapor and liquid, $\mu_g - \mu_l$, is comparable to the energy of typical thermal fluctuations, of the order of $k_B T$. The structure of a surface-induced interface in such a fluid is likely not to differ significantly from that of the interface exactly at coexistence. We show in section II B that, for both the SPC and SPC/E models at room temperature and 1 atm pressure, γ and $\tilde{\gamma}$ are essentially indistinguishable, as Stillinger imagined.[5] Work from our group[18] suggested that γ and $\tilde{\gamma}$ should differ slightly. This suggestion, we shall see, is the result of an incomplete analysis of the asymptotic behavior of $\Delta\mu(R)$.

The length-scale dependence of hydrophobicity we have described is in fact a general feature of solvophobic solvation in dense liquids with intermolecular attractions. "Solvophobic" refers to the general case of a solute which attracts solvent molecules less strongly than solvent molecules attract one another. Indeed, the onset of drying with increasing solute size has been demonstrated in simulations of hard sphere solutes in a Lennard-Jones (LJ) fluid.[18] In section III, we take advantage of the computational simplicity of the LJ fluid to examine the crossover in $\Delta\mu(R)$ for thermodynamic states at and near coexistence [i.e., $(\mu_g - \mu_l)/k_B T \lesssim 1$] that are away from the triple point but still far from the critical point. As in the case of water at ambient conditions, we find that $\tilde{\gamma}$ for these states, suitably corrected for nonnegligible vapor density, is virtually indistinguishable from γ.

II. Solvation in Water

A. Solvation of Spherical Cavities. We have determined $\Delta\mu(R)$ for hard sphere solutes, with radii $0 \leq R \leq 10.25$ Å, by

---

Scaling of Hydrophobic Solvation Free Energies

J. Phys. Chem. B, Vol. 105, No. 28, 2001 **6705**

computing the distribution of cavity sizes in water at equilibrium:[10]

$$\Delta\mu(R) = -k_B T \ln[\int_R^\infty dR' \, P(R')] \quad (1)$$

In eq 1, $P(R)$ is the probability that the largest hard sphere solute that may be inserted at the origin has radius R, k_B is Boltzmann's constant, and T is temperature. Because the spontaneous formation of large cavities is extremely unlikely, we use umbrella sampling[19] to compute $P(R)$ in Monte Carlo simulations. Specifically, $P(R)$ is determined for several overlapping windows, $R_{min} < R < R_{max}$, of width 0.6−1.0 Å. In each window, a bias potential is applied to achieve nearly uniform sampling of cavity sizes. The unbiased distribution is then constructed over the entire range of R using the multiple histogram method,[20] which minimizes the variance in the computed distribution while ensuring that $P(R)$ is continuous. By allowing the system to equilibrate subject to a sequence of constraints corresponding to successively larger solute radii, we in effect calculate the reversible work to grow large cavities. Most simulations were carried out with 864 molecules. No noticeable differences were observed when calculations of $P(R)$ were repeated for the largest R with 2048 molecules.

Our simulations were performed at constant pressure. This feature is crucial, because drying at the solute's surface is accompanied by significant volume fluctuations of the central simulation cell. A constraint of constant volume would inhibit these fluctuations and, therefore, artificially prevent the possibility of drying. The thermodynamic states defined by the applied pressure (1 atm) and temperature (298 K) in our simulations mimic ambient conditions and have been found,[21] for both water models considered, to be about as close to coexistence as real water. Specifically, $(\mu_g - \mu_l)/k_B T \approx \ln(p/p_{coex})$ is 3.5 for real water, 4.6 for the SPC/E model, and 3.5 for the SPC model. Here, p_{coex} is the liquid−vapor coexistence pressure at temperature T.

The intermolecular potentials in both the SPC and SPC/E models consist of Coulomb and LJ interactions. The Coulomb interactions are treated by Ewald summation, which properly accounts for their long-ranged nature. The LJ interactions are truncated at a distance, r_c, of half the simulation cell length and shifted to preserve continuity of the potential. Although this truncation should not significantly influence the ensemble of configurations we sample, the omitted attractive tail, $u_t(r)$, of the LJ potential does make a significant contribution to $\Delta\mu(R)$. We compute this contribution using first order thermodynamic perturbation theory:

$$\Delta\mu_{tail}(R) = \frac{1}{2}[\int_{\langle V\rangle_R} d\mathbf{r}_1 \int_{\langle V\rangle_R} d\mathbf{r}_2 \, \rho^{(2)}(\mathbf{r}_1,\mathbf{r}_2,\langle V\rangle_R)u_t(r_{12}) -$$
$$\int_{\langle V\rangle_0} d\mathbf{r}_1 \int_{\langle V\rangle_0} d\mathbf{r}_2 \, \rho^{(2)}(\mathbf{r}_1,\mathbf{r}_2,\langle V\rangle_0)u_t(r_{12})] \quad (2)$$

$$\approx 4\pi^2 \int_R^\infty dr \, r^2 \int_0^\infty dr' \, r'^2 u_t(r')g^{(0)}(r') \times$$
$$\int_{-1}^1 ds \, [\rho(r)\rho([r^2 + r'^2 + 2rr's]^{1/2}) - \rho_l^2] \quad (3)$$

Here, $\rho^{(2)}(\mathbf{r}_1,\mathbf{r}_2,\langle V\rangle)$ is the joint probability that a particular water molecule is located at $\mathbf{r}_1$ and a second water molecule is simultaneously located at $\mathbf{r}_2$, for a system of average volume $\langle V\rangle$. In eq 2, $\langle V\rangle_R$ is the average volume of the system containing a solute of radius R. We arrive at eq 3 by assuming that the pair density, $\rho^{(2)}(\mathbf{r}_1,\mathbf{r}_2)$, can be decomposed into a product of the single particle densities, $\rho(r_1)$ and $\rho(r_2)$, and the pair correlation function, $g^{(0)}(|\mathbf{r}_1 - \mathbf{r}_2|)$, of the uniform liquid with

density ρ_l.[22] We further assume that the fluid is incompressible, i.e., $\langle V\rangle_R - \langle V\rangle_0 \approx 4\pi R^3/3$. On the basis of the changes in volume with cavity size in our simulations, this assumption of incompressibility appears to be quite accurate. In the planar limit, $R \rightarrow \infty$, the expression for $\Delta\mu_{tail}(R)/(4\pi R^2)$ in eq 3 is consistent with the tail correction expression due to Blokhuis et al.[23] for the surface tension of a liquid−vapor interface. This correspondence results from approximating the density profile by a step function, $\rho(\mathbf{r}) = \rho_l\theta(r - R)$, and assuming $g^{(0)}(r) = 1$ for $r > r_c$.

The excess solvation free energy per surface area is plotted in Figure 1a for both the SPC and SPC/E models. As expected from theory,[1−3] $\Delta\mu(R)/(4\pi R^2)$ scales approximately with R for small R. Results for the two models are nearly identical for $R < 2.5$ Å. Such small solutes may be accommodated by the solvent through small rearrangements, so that $\Delta\mu(R)$ is largely entropic. Although the solute reduces the volume of configuration space available to the solvent, large energetic penalties corresponding to broken hydrogen bonds are not incurred. Differences between the two models at this length scale are nearly proportional to the roughly 2% difference in bulk density. At a microscopic radius of about 5 Å, $\Delta\mu(R)/(4\pi R^2)$ crosses over to a weaker R dependence. Quantitative results for the two models deviate strongly beyond this crossover. Large solutes have a disruptive effect on the hydrogen bond network, and the free energetics become dominated by the strength of these interactions. In this regime, solvation is more costly in the SPC/E model, reflecting in part the difference in surface tensions for the two models (see Table 1).

To obtain a surface tension of the solute−solvent interface in the limit $R \rightarrow \infty$, we assume that

$$\frac{\Delta\mu(R)}{4\pi R^2} \approx \frac{pR}{3} + \tilde{\gamma}\left(1 - \frac{2\delta}{R}\right) \quad (4)$$

as in scaled particle theory.[24,25] The first term on the right-hand side of eq 4 is the work to expand a cavity against the external pressure, p. Because of water's proximity to the triple point at room temperature, the applied pressure in our simulations is very small, and this contribution to the free energy is significant only for extremely large solute volumes. The second term on the right-hand side of eq 4 describes the work due to surface tension, including the leading term in an expansion in powers of $1/R$. For a macroscopic surface, the coefficient δ is the Tolman length, which determines the free energetics of interfacial curvature.[26] In our analysis of microscopic solutes, δ describes the approach to an asymptotic scaling of $\Delta\mu$ with surface area and need not correspond to the Tolman length. The curves in Figure 1a were fit to eq 4 for radii R between 6.0 and 10.25 Å. The resulting values of $\tilde{\gamma}$ and δ are given in Table 1.

Our simulation data suggest that the large-solute limit, in which $\Delta\mu$ is proportional to the area $A = 4\pi R^2$ of the interface between solvent and solute, is approached slowly. It has been suggested, however, that this proportionality may hold even for small solutes if a different choice is made for the interfacial area, $\tilde{A} = 4\pi(R - R_s)^2$.[27] Here, $R_s = 1.4$ Å is the approximate radius of a water molecule. To test this idea, we have plotted $\Delta\mu/4\pi(R - R_s)^2$ in Figure 1a as a function of R. With this alternative choice of the solvent−solute dividing surface, the range of R for which $\Delta\mu \propto \tilde{A}$ clearly does not extend to $R < 1$ nm. This choice also does not significantly change the extrapolation of our data, yielding an estimate of $\tilde{\gamma}$ that differs by less than 5% from the value given in Table 1.

The radial distribution function about the solute, $g(r)$, from simulation and the theory of solvation due to Lum, Chandler,
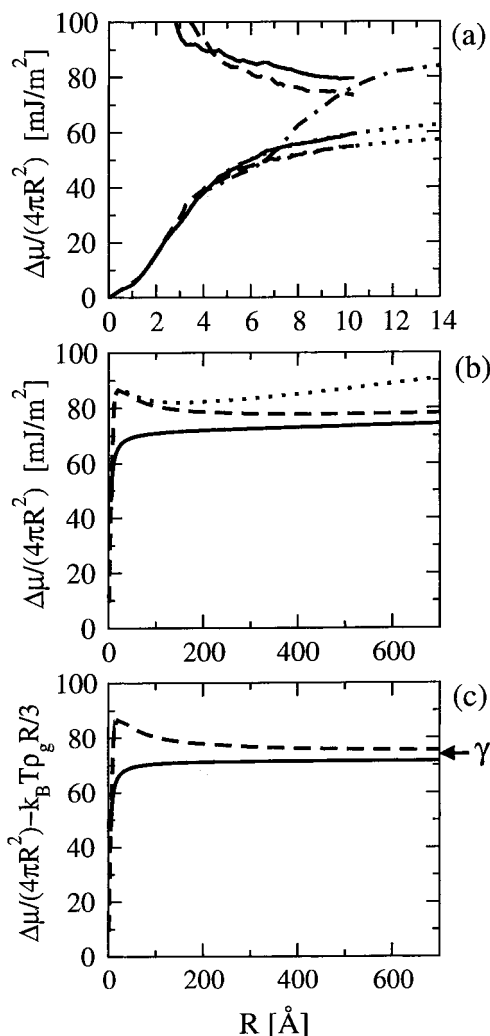
Figure 1. (a) Excess chemical potential per surface area, $\Delta\mu(R)/(4\pi R^2)$, including tail correction, $\Delta\mu_{\text{tail}}(R)$, for a solute of radius R in water at 298 K and 1.0 atm for the SPC/E (lower solid line) and SPC (lower dashed line) models. The dotted lines are the results of the regression analysis using eq 4. The dot−dashed line is the LCW theory prediction of the free energy for SPC/E water, $\Delta\mu_{\text{LCW}}(R)/(4\pi R^2)$. The upper solid curve (SPC/E model) and upper dashed curve (SPC model) show $\Delta\mu(4\pi(R-R_s)^2)$, where R_s is 1.4 Å, reflecting a different choice of solute−solvent dividing surface. (b and c) The large R behavior of the regression line for SPC/E water (solid line), $\Delta\mu_{\text{LCW}}(R)/(4\pi R^2)$ (dotted line), and $\Delta\tilde{\mu}_{\text{LCW}}(R)/(4\pi R^2)$ (dashed line). (See the text for descriptions of these quantities.) The arrow in c indicates the value of the liquid−vapor surface tension, γ. The simulation curves were calculated from data collected every five simulation cycles until an average of approximately 10 000 points were collected in each histogram bin (of width 0.1 Å), after equilibrating for 40 000 steps. The statistical error in the free energy was estimated from the variance of block averages.[19] Simulations in each window were carried out in blocks of 40 000 Monte Carlo cycles (apparently sufficient for data from adjacent blocks to be uncorrelated). The block average of the free energy was constructed using data from one block in each window. The standard deviation is approximately 1.0 mJ/m² for almost all of the points along the curves. The tail correction, $\Delta\mu_{\text{tail}}(R)$, was obtained from eq 3 for the full range of R by assuming $\rho(r) \approx \rho_l\theta(r - R)$ and $g^{(0)} \approx 1$. Almost identical results were obtained using calculated density profiles, $\rho(r)$, for $R = 2, 4, 6, 8,$ and 10 Å, and the oxygen−oxygen pair correlation function, $g^{(0)}(r)$, from a simulation of the uniform liquid. $\Delta\mu_{\text{tail}}(R)/(4\pi R^2)$ is approximately 1.5 mJ/m² for the largest R.

TABLE 1: Surface Tension of the Liquid−Vapor Interface, γ, and Effective Surface Tension, $\tilde{\gamma}$, and Tolman Length, δ, of a Hard Sphere Solute, Calculated for the SPC and SPC/E Water Models

fluid	T [K]	p [atm]	γ^a [mJ/m²]	$\tilde{\gamma}^b$ [mJ/m²]	δ^b [mJ/m²]
SPC	298.0	1.0	65.3 ± 2	64.2 ± 0.8	0.76 ± 0.05
SPC/E	298.0	1.0	73.6 ± 2	71.8 ± 0.8	0.90 ± 0.03

a Calculated in liquid−vapor interface simulations 2 ns in length. Systems were allowed to equilibrate for 1 ns, after which the density profile and components of the pressure tensor fluctuated around mean values. Statistical error was determined by computing the distribution of instantaneous values of γ and estimating the number of independent observations from the decay of time correlation functions. *b* Regression coefficients obtained using a general linear least squares procedure, which uses both the values and the estimated statistical error of the data points. The error was taken as the square root of the diagonal elements of the covariance matrix.[36] Values of R used in the regression were chosen to be sufficiently large that the asymptotic expression in eq 4 is valid but covering a wide enough range that the error in $\tilde{\gamma}$ is smaller than that in γ.
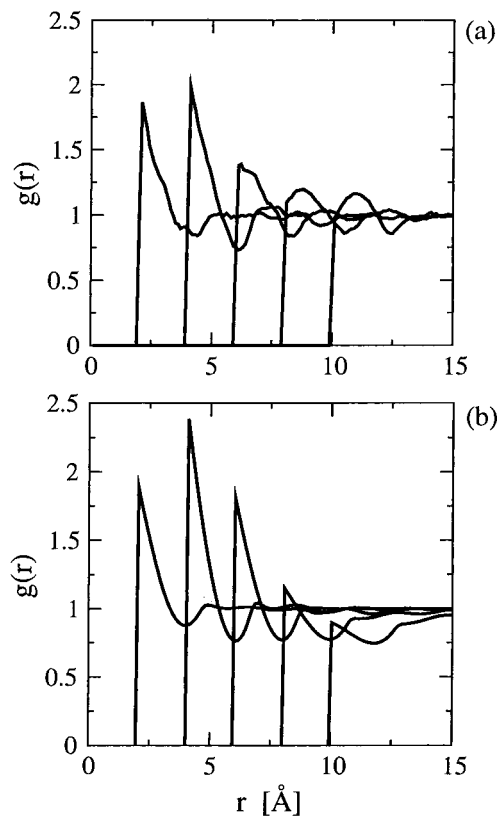

Figure 2. Radial distribution function, $g(r)$, as a function of distance r from the solute center for solutes with radii $R = 2.0, 4.0, 6.0, 8.0,$ and 10.0 Å, in SPC/E water at 298 K and 1.0 atm from (a) simulation and (b) LCW theory.

and Weeks (LCW),[1] is plotted in Figure 2 for several solute sizes in SPC/E water.[28] The simulation and theory curves show similar behavior. The density at contact, $g(R)$, increases initially with R because of the packing of solvent molecules around the solute. For $R > 4$ Å, $g(R)$ decreases monotonically as the unbalanced attractive force from the bulk grows in magnitude.[1] For the largest solute size we have studied by simulation, $R = 10$ Å, a drying interface is beginning to nucleate, i.e., $g(R) < 1$.

B. Surface Tension of a Free Liquid−Vapor Interface. To interpret the planar limit of hard sphere solvation, we have computed the liquid−vapor surface tensions, γ, of the SPC and SPC/E water models at 298 K. This calculation is accomplished in molecular dynamics simulations by constraining the total density so that the system lies in the two-phase region. With this constraint, a slab of liquid forms in the simulation cell, minimizing the area of interfaces between liquid and vapor. The surface tension may then be computed through the difference

Scaling of Hydrophobic Solvation Free Energies

J. Phys. Chem. B, Vol. 105, No. 28, 2001 **6707**

TABLE 2: Surface Tension of the Liquid−Vapor Interface, γ, and Effective Surface Tension, $\tilde{\gamma}$, and Tolman Length, δ, of a Hard Sphere Solute, Calculated for Three Examples of the LJ Fluid

fluid	$T\,[\epsilon/k_B]$	$p\,[\epsilon/\sigma^3]$	$\gamma^a\,[\epsilon/\sigma^2]$	$\tilde{\gamma}^b\,[\epsilon/\sigma^2]$	$\delta^b\,[\sigma]$	$\tilde{\gamma}_c{}^b\,[\epsilon/\sigma^2]$	$\tilde{\delta}_c{}^b\,[\sigma]$
LJ-1	0.701	0.0050	0.67 ± 0.04	0.69 ± 0.01	-0.17 ± 0.04	0.66 ± 0.01	-0.21 ± 0.04
LJ-2	0.836	0.020	0.37 ± 0.04	0.42 ± 0.01	-0.57 ± 0.05	0.37 ± 0.01	-0.69 ± 0.06
LJ-3	0.836	0.025		0.42 ± 0.02	-0.59 ± 0.09	0.36 ± 0.02	-0.73 ± 0.10

[a] Calculated in liquid−vapor interface simulations of length 250 000 elementary LJ time steps, τ, after equilibrating for 50 000 τ. Statistical error determined as described in Table 1. [b] Defined in eqs 4 and 5 and obtained by regression for $4.5 < R < 5.5\sigma$, as described in Table 1.

of pressure tensor components normal and tangential to the interface.[30] In these simulations, LJ interactions were truncated and shifted at 9.8 Å. The tail correction to γ was computed using eq 5 of ref 23. Simulations were carried out for 512 water molecules in a simulation cell with dimensions 19.7 × 19.7 × 100 Å.

The calculated values of γ are given in Table 1. The SPC/E value differs by only a few percent from an extrapolation of the results of Alejandre et al.[31] for a similar model with flexible molecular geometry. The results for γ are consistent with the values of $\tilde{\gamma}$ computed in the cavity simulations for both water models. This correspondence reflects the proximity of both systems to coexistence. It also indicates that the contributions of interfacial fluctuations are relatively weak. Transverse fluctuations are permitted for a free liquid−vapor interface but are hindered in the case of hard sphere solvation by the presence of a rigid boundary. If fluctuations of the free interface were large enough to make a significant entropic contribution to the interfacial free energy, then their hindrance would lead to a noticeable difference between γ and $\tilde{\gamma}$.

III. Solvation in the LJ Fluid

The simulations of aqueous solvation described above are computationally very expensive and would be time-consuming to repeat at a variety of thermodynamic states. To investigate solvation behavior outside the neighborhood of the triple point, we have instead performed analogous simulations of a LJ fluid. We consider three thermodynamic states, denoted LJ-1, LJ-2, and LJ-3. (Thermodynamic conditions are given in Table 2.) For the fluid we simulate, in which interactions are truncated and shifted at 2.5σ, the first two states are at coexistence. LJ-1 lies close to the triple point, and LJ-2 is approximately a third of the way between the triple and critical points.[32] The last state is close to, but quantitatively away from, coexistence, as measured by $(\mu_g - \mu_l)/k_BT \approx \ln(p/p_{coex}) = 0.22$.[32] For comparison, we have also computed the liquid−vapor surface tension at coexistence for the same temperatures.

Hard sphere solvation simulations were carried out with 2048 LJ solvent particles for $0 \leq R \leq 4.1\sigma$ and 4000 solvent particles for $3.5\sigma \leq R \leq 5.5\sigma$. We repeated these calculations with 6912 solvent particles for $5.0\sigma \leq R \leq 5.5\sigma$ and found no significant dependence on system size. Slab simulations involved 1024 particles in simulation boxes with dimensions $6.84\sigma \times 6.84\sigma \times 40.0\sigma$ at $T^* = 0.701$ and $6.84\sigma \times 6.84\sigma \times 50.0\sigma$ at $T^* = 0.836$.

Results for these LJ fluids (see Figure 3 and Table 2) differ from those for water in two important respects. First, the crossover to drying occurs for much smaller hard sphere solutes than in water (relative to the solvent diameter, which is roughly 2.8 Å, for water). Correspondingly, density depletion at contact with the solute occurs for much smaller solutes for the LJ fluid[18] than observed in Figure 2 for water. The relatively slower approach to drying for water is expected because of the strong energetic preference for maintaining hydrogen bond networks.

Second, the surface tension of a planar solute, $\tilde{\gamma}$, as defined in eq 4, does not closely match the liquid−vapor surface tension,
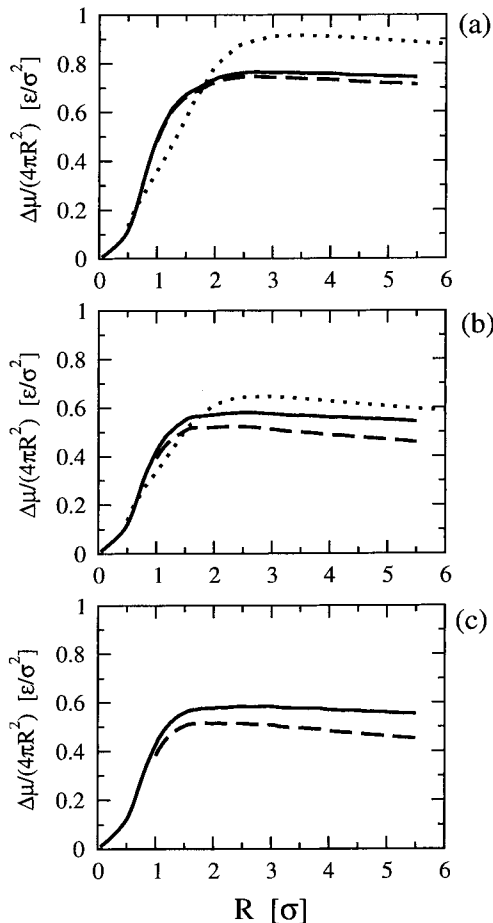

Figure 3. Excess chemical potential per surface area, $\Delta\mu(R)/(4\pi R^2)$, for a solute of radius R in the LJ fluid at three thermodynamic states: (a) LJ-1, (b) LJ-2, and (c) LJ-3 (solid lines). See Table 2 for definitions of these states. $\Delta\mu(R)/(4\pi R^2) - \Delta\mu_{g\rightarrow 0}(R)/(4\pi R^2)$ is also plotted for (a) LJ-1, (b) LJ-2, and (c) LJ-3 (dashed lines). Curves were constructed from data collected in simulations in which approximately 15 000 points were obtained in each histogram bin (width 0.05σ). The standard deviation is $0.5-1.0 \times 10^{-2}$ for almost all of the points along the curves. Values of $\Delta\mu(R)/(4\pi R^2)$ from the LCW theory are also shown for the (a) LJ-1 and (b) LJ-2 states (dotted lines).

γ, for the states LJ-2 and LJ-3. A simple argument accounts for this discrepancy quantitatively. The first term on the right-hand side of eq 4 describes the free energy obtained by replacing a hard sphere solute with an ideal vapor of the same volume. The contribution $pR/3$ is appropriate for a rarefied gas, such as water vapor at 298 K. The vapor phases for LJ-2 and LJ-3, however, have densities, ρ_g, that are 4% and 5% of the bulk liquid density, respectively. At these densities, the gases are significantly nonideal. A more appropriate asymptotic expression for these states is

$$\frac{\Delta\mu(R)}{4\pi R^2} \approx \frac{\Delta\mu_{g\rightarrow 0}}{4\pi R^2} + \tilde{\gamma}_c\left(1 - \frac{2\delta_c}{R}\right) \qquad (5)$$

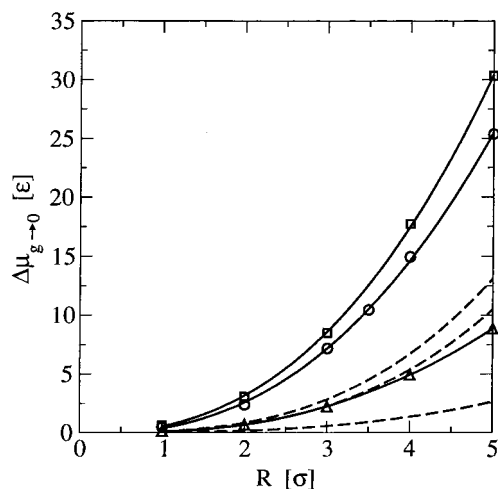where $\Delta\mu_{g\rightarrow 0}$ is the reversible work to change the gas density

Figure 4. Change in excess free energy, $\Delta\mu_{g\rightarrow 0}$, upon evacuating a volume with average density equal to the vapor density to obtain an empty cavity, for the three LJ fluids studied: LJ-1 (triangles), LJ-2 (circles), and LJ-3 (squares). The solid lines are cubic functions fitted to the data. The dashed lines, in ascending order, are $4\pi p R^3/3$ with $p\sigma^3/\epsilon = 0.0050$, 0.020, and 0.025, corresponding to the applied pressures for LJ-1, LJ-2, and LJ-3, respectively.

in the volume v from ρ_g to zero. Only for an ideal gas is this work pv. To account for deviations from this ideal behavior, we have computed $\Delta\mu_{g\rightarrow 0}$ using umbrella sampling[19] in precisely the way described in ref 18. The results are plotted in Figure 4 for each of the LJ fluids. These results reflect strong nonideality. For $R = 5\sigma$, $\Delta\mu_{g\rightarrow 0}$ is 6ϵ, 15ϵ, and 17ϵ larger than the ideal gas result for LJ-1, LJ-2, and LJ-3, respectively. The data shown in Figure 4 were fit to a cubic equation in R to obtain $\Delta\mu_{g\rightarrow 0}$ for all R. The corrected surface tension, $\tilde{\gamma}_c$, then obtained by fitting $\Delta\mu(R)/(4\pi R^2)$ to the asymptotic form in eq 5, is nearly identical to the liquid−vapor surface tension, γ, at the same temperature, even for the state away from coexistence (see Table 2). As in the case of water, for the LJ states we have considered, interfacial structure, and fluctuations near a planar solute appear to be very similar to those of a free liquid−vapor interface.

We have compared our simulations with the LCW theory[1] by including the theoretical predictions of $\Delta\mu(R)/(4\pi R^2)$ in Figures 1 and 3. For both water and the LJ fluid,[28] the theory gives a reasonable prediction of the crossover but overestimates the free energy for solute radii beyond the crossover. For the case of water, some of the differences between theory and simulation have trivial origins that are easily corrected. In particular, to a good approximation, the vapor phase of water at 298 K and 1 atm is an ideal gas, for which density fluctuations obey Poisson statistics, and hence, $\Delta\mu_{g\rightarrow 0}$ should be $k_BT\rho_g v = pv$. Gaussian statistics used in the LCW theory, however, predict this reversible work to be a factor of 2 smaller, i.e., $k_BT\rho_g v/2$. In addition, the simple two parameter equation of state that has been used when applying the LCW theory to water[1] predicts a value for the vapor density, $\rho_{g,LCW}$, which is much smaller than the liquid density but still a factor of 10 larger than the actual ρ_g. (In the LJ solvent case, we have used a more accurate equation of state[32] that avoids this error.) As such, the LCW prediction for very large hard spheres in water, $\Delta\mu_{LCW}(R)$, can be improved by replacing it with

$$\frac{\Delta\tilde{\mu}_{LCW}(R)}{4\pi R^2} \approx \frac{\Delta\mu_{LCW}(R)}{4\pi R^2} + \frac{k_BTR}{3}\left(\rho_g - \frac{\rho_{g,LCW}}{2}\right) \quad (6)$$

$\Delta\tilde{\mu}_{LCW}(R)/(4\pi R^2)$ and $\Delta\mu_{LCW}(R)/(4\pi R^2)$ are plotted along with the extrapolated simulation results in Figure 1b. Figure 1c shows

that the large R limit of $\Delta\tilde{\mu}_{LCW}(R)/(4\pi R^2) - k_BT\rho_g R/3$ approaches a surface free energy, $\tilde{\gamma}_{LCW}$, that is nearly identical to that of the extrapolated simulation result, $\tilde{\gamma} \approx \gamma$. However, the two results approach this large R limit differently.

In our previous work,[18] the asymptotic behavior of $\tilde{\gamma}$ was deduced from a visual inspection of graphs such as Figure 3, rather than the extrapolations given by eqs 4 and 5. The conclusion in that work that γ and $\tilde{\gamma}$ differ is incorrect, because of the very slow approach of $\Delta\mu(R)/(4\pi R^2)$ to the $R \rightarrow \infty$ limit. The magnitude of δ is a measure of the approach to this limit. In our calculations, δ is negative for all three LJ fluids and is positive for the SPC and SPC/E water models. The correct sign of δ for these systems in the thermodynamic limit (the Tolman length) has not been unambiguously determined and is a matter of controversy.[33,34] Interestingly, the magnitude of our values, fractions of the solvent diameter, are consistent with previously reported values of the Tolman length.[35]

References and Notes

(1) Lum, K.; Chandler, D.; Weeks, J. D. *J. Phys. Chem. B* **1999**, *103*, 4570.

(2) Hummer, G.; Garde, S.; García, A. E.; Pohorille, A.; Pratt, L. R. *Proc. Natl. Acad. Sci. U.S.A.* **1996**, *93*, 8951.

(3) Pratt, L. R.; Chandler, D. *J. Chem. Phys.* **1977**, *67*, 3683.

(4) Chandler, D. *Phys. Rev. E* **1993**, *48*, 2898.

(5) Stillinger, F. H. *J. Solution Chem.* **1973**, *2*, 141.

(6) Huang, D. M.; Chandler, D. *Proc. Natl. Acad. Sci. U.S.A.* **2000**, *97*, 8324.

(7) Berendsen, H. J. C.; Postma, J. P. M.; van Gunsteren, W. F.; Hermans, J. In *Intermolecular Forces*; Pullmann, B., Ed.; Reidel: Dordrecht, The Netherlands, 1981; p 331.

(8) Berendsen, H. J. C.; Grigera, J. R.; Straatsma, T. P. *J. Phys. Chem.* **1987**, *91*, 6269.

(9) Hummer, G.; Garde, S. *Phys. Rev. Lett.* **1998**, *80*, 4193.

(10) Pohorille, A.; Pratt, L. R. *J. Am. Chem. Soc.* **1990**, *112*, 5066.

(11) Pratt, L. R.; Pohorille, A. *Proc. Natl. Acad. Sci. U.S.A.* **1992**, *89*, 2995.

(12) Ikeguchi, M.; Shimizu, S.; Nakamura, S.; Shimizu, K. *J. Phys. Chem. B* **1998**, *102*, 5891.

(13) Matubayasi, N.; Nakahara, M. *J. Chem. Phys.* **2000**, *112*, 8089.

(14) Prévost, M.; Oliveira, I. T.; Kocher, J. P.; Wodak, S. J. *J. Phys. Chem.* **1996**, *100*, 2738.

(15) Tomás-Oliveira, I.; Wodak, S. J. *J. Chem. Phys.* **1999**, *111*, 8576.

(16) Beutler, T. C.; Béguelin, D. R.; van Gunsteren, W. F. *J. Chem. Phys.* **1995**, *102*, 3787.

(17) Floris, F. M.; Selmi, M.; Tani, A.; Tomasi, J. *J. Chem. Phys.* **1997**, *107*, 6353.

(18) Huang, D. M.; Chandler, D. *Phys. Rev. E* **2000**, *61*, 1501.

(19) Frenkel, D.; Smit, B. *Understanding Molecular Simulation: From Algorithm to Applications*; Academic Press: San Diego, CA, 1996; Chapter 7.

(20) Ferrenberg, A. M.; Swendsen, R. H. *Phys. Rev. Lett.* **1989**, *63*, 1195.

(21) Errington, J. R.; Panagiotopoulos, A. Z. *J. Phys. Chem. B* **1998**, *102*, 7470.

(22) To test the decomposition approximation in eq 3 for correlations near the solute, we have computed contributions to $\Delta\mu_{tail}(R)$ for $r_1 < L/2$ and $r_2 < L/2$ directly from our cavity simulations. Here, L is the dimension of our central simulation cell. For $R = 2$ Å, the directly computed contribution differs from that computed using eq 3 by 15% of $\Delta\mu_{tail}(R)$. For $R = 4$, 6, 8, and 10 Å, this difference is negligible (less than 1% of $\Delta\mu_{tail}(R)$).

(23) Blokhuis, E. M.; Bedeaux, D.; Holcomb, C. D.; Zollweg, J. A. *Mol. Phys.* **1995**, *85*, 665.

(24) Reiss, H.; Frisch, H. L.; Lebowitz, J. L. *J. Chem. Phys.* **1959**, *31*, 369.

(25) Reiss, H.; Frisch, H. L.; Helfand, E.; Lebowitz, J. L. *J. Chem. Phys.* **1960**, *32*, 119.

(26) Tolman, R. C. *J. Chem. Phys.* **1949**, *17*, 333.

(27) Ashbaugh, H. S.; Kaler, E. W.; Paulaitis, M. E. *J. Am. Chem. Soc.* **1999**, *121*, 9243.

Scaling of Hydrophobic Solvation Free Energies

J. Phys. Chem. B, Vol. 105, No. 28, 2001 **6709**

(28) The LCW theory was implemented for the SPC/E model using the same method given in ref 1 for real water and for the LJ fluid using the method in ref 18. The properties of the SPC/E model required by the theory were obtained either directly from our simulations or from previous studies.[21,29]

(29) Motakabbir, K. A.; Berkowitz, M. *J. Phys. Chem.* **1990**, *94*, 8359.

(30) Kirkwood, J. G.; Buff, F. P. *J. Chem. Phys.* **1949**, *17*, 338.

(31) Alejandre, J.; Tildesley, D. J.; Chapela, G. A. *J. Chem. Phys.* **1995**, *102*, 4574.

(32) Johnson, J. K.; Zollweg, J. A.; Gubbins, K. E. *Mol. Phys.* **1993**, *78*, 591.

(33) Blokhuis, E. M.; Bedeaux, D. *J. Chem. Phys.* **1992**, *97*, 3576.

(34) van Geissen, A. E.; Blokhuis, E. M.; Bukman, D. J. *J. Chem. Phys.* **1998**, *108*, 1148.

(35) Haye, M. J.; Bruin, C. *J. Chem. Phys.* **1994**, *100*, 556.

(36) Press, W. H.; Teukolsky, S. A.; Vetterling, W. T.; Flannery, B. P. *Numerical Recipes in C—The Art of Scientific Computing*, 2nd ed.; Cambridge University Press: Cambridge, U.K., 1992; Chapter 15.